

One-step preparation of N-doped graphitic layer encased cobalt / iron carbide nanoparticles derived from cross-linked polyphthalocyanines as highly active electrocatalysts towards the oxygen reduction reaction

*Zhengping Zhang, Shaoxuan Yang, Meiling Dou, Jing Ji, and Feng Wang**

State Key Laboratory of Chemical Resource Engineering, Beijing Key Laboratory of Electrochemical Process and Technology for Materials, Beijing University of Chemical Technology, Beijing 100029, China.

E-mail: wangf@mail.buct.edu.cn

Experimental section

Materials

CoCl₂·6H₂O, FeCl₂, urea, NH₄Cl, (NH₄)₂Mo₂O₇, phthalic anhydride acid, pyromellitic dianhydride, acetone, methanol, ethanol, KOH were purchased from Sinopharm. 5% Nafion were bought from DuPont, respectively. High-purity argon gas was provided from Beijing AP BAIF Gases Industry Co., Ltd. All chemicals were of analytical grade and applied without further purification. Distilled ultrapure water was used for all solution preparation and cleaning products.

Characterization and Electrochemical measurements

Solid-state NMR spectra were measured on a Bruker AV300 spectrometer operating at 75.5 MHz for ¹³C. Scanning electron microscopy (SEM) images of the products were obtained using a JEOL FE-JSM-6701F field emission scanning electron microscope. Transmission electron microscopy (TEM) images of the products were obtained by a JEOL JEM-2010. All X-ray photoelectron spectroscopy (XPS) analysis was obtained using ThermoFisher Scientific ESCALAB 250 and ASAP 2020 analyser charging referenced to the C 1s XPS peak (284.1 eV). The X-ray diffraction profile (XRD) was obtained on a Rigaku D/Max 2500 VB2+/PC diffractometer with Cu K α radiation ($\lambda = 1.54056 \text{ \AA}$) as the X-ray source. The differential thermal analysis (DTA) was obtained on a Rigaku TG-8120 in the air atmosphere with the heating rate of 5 K min⁻¹.

Raman spectroscopy was obtained using a Horiba Jobin Yvon LabRam HR800 with an excitation wavelength of 532 nm.

Electrochemical measurements were obtained with PINE and CHI-760e. All electrochemical measurements were carried out in a single compartment glass cell at room temperature. A potassium chloride saturated calomel reference electrode (SCE) and a Pt wire counter electrode were used together with the modified glassy carbon (GC) working electrode. 10 mg of the electrocatalyst was dispersed with a mixture of 2 mL ethanol and 5 μ L 5 % Nafion solutions before sonicated. The catalyst ink was transferred onto the polished GC electrode and dried for 20 min at room temperature. Commercial 20 wt.% Pt/C (Johnson Matthey, UK) catalyst obtained from Alfa Aesar was used for comparison. The loading mass as-prepared electrocatalysts on the working electrode is 0.4 mg cm⁻², and that of the Pt/C catalysts is 0.2 mg cm⁻².

Rotating disk electrode (RDE) measurements

The glassy carbon rotating disk electrode is 4 mm in diameter. The Koutecky–Levich (K-L) plots reflecting the relation of I^{-1} vs. $\omega^{-1/2}$ were constructed according to:

$$I^{-1} = i_k^{-1} + (0.2nFC_{O_2}D_{O_2}^{2/3}\gamma^{-1/6})^{-1}\omega^{-1/2}$$

where I is the measured current, i_k is the kinetic-limiting current, n is the number of electrons transferred per oxygen molecule, F is the Faraday constant (96,500 C mol⁻¹), C_{O_2} is the concentration of oxygen in 0.1 M KOH, D_{O_2} is the diffusion coefficient of oxygen in 0.1 M KOH, γ is the kinematic viscosity of the 0.1 M KOH and ω is the electrode rotation rate.

For the Tafel plot, the kinetic current was calculated from the mass-transport correction of RDE by:

$$J_k = \frac{J \times J_L}{J_L - J}$$

Rotating ring-disk electrode (RRDE) measurements

The disk electrode was scanned cathodically at a rate of 5 mV·s⁻¹ and the ring potential were constant at 1.5 V vs. RHE. The electron transfer number (n) was determined by the followed equation:

$$n = 4 \times \frac{I_d}{I_d + I_r/N}$$

where I_d is disk current, I_r is ring current and $N = 0.4$ is the current collection efficiency of the Pt ring. The peroxide percentage (% HO_2^-) was calculated based on the equation:

$$\%HO_2^- = 200 \times \frac{I_r/N}{I_d + I_r/N}$$

Table S1 Elements contents derived from XPS measurements of P-CoPc and P-CoPPc-XL.

		P-CoPc	P-CoPPc-LXL	P-CoPPc-MXL	P-CoPPc-HXL
Elements (at. %)	C	84.17	89.69	90.09	81.68
	O	11.44	6.16	5.15	8.56
	N	1.43	3.43	4.33	9.13
	Co	2.95	0.73	0.43	0.64

Table S2 Elements contents derived from XPS measurements of P-FePc and P-FePPc-XL.

		P-FePc	P-FePPc-LXL	P-FePPc-MXL	P-FePPc-HXL
Elements (at. %)	C	89.97	89.93	83.11	75.77
	O	5.86	4.60	6.98	9.18
	N	3.94	5.21	9.41	14.44
	Fe	0.23	0.27	0.50	0.61

Table S3 Composition analysis of elements Co and Fe in P-TMPc and P-TMPPc-HXL.

Detectable Element	Co		Fe	
Sample	P-CoPc	P-CoPPc-HXL	P-FePc	P-FePPc-HXL
Unit	ppm	ppm	ppm	ppm
Average Value	19.52	17.74	20.18	15.92
Standard Deviation	0.33	0.30	0.24	0.28
%RSD	1.671	2.45	1.12	1.51
Rep#1	19.75	17.67	20.01	15.96
Rep#2	19.29	17.80	20.35	15.87
Calculation ($\mu\text{g}/100\text{ g}$)	67.44	62.14	68.12	57.79

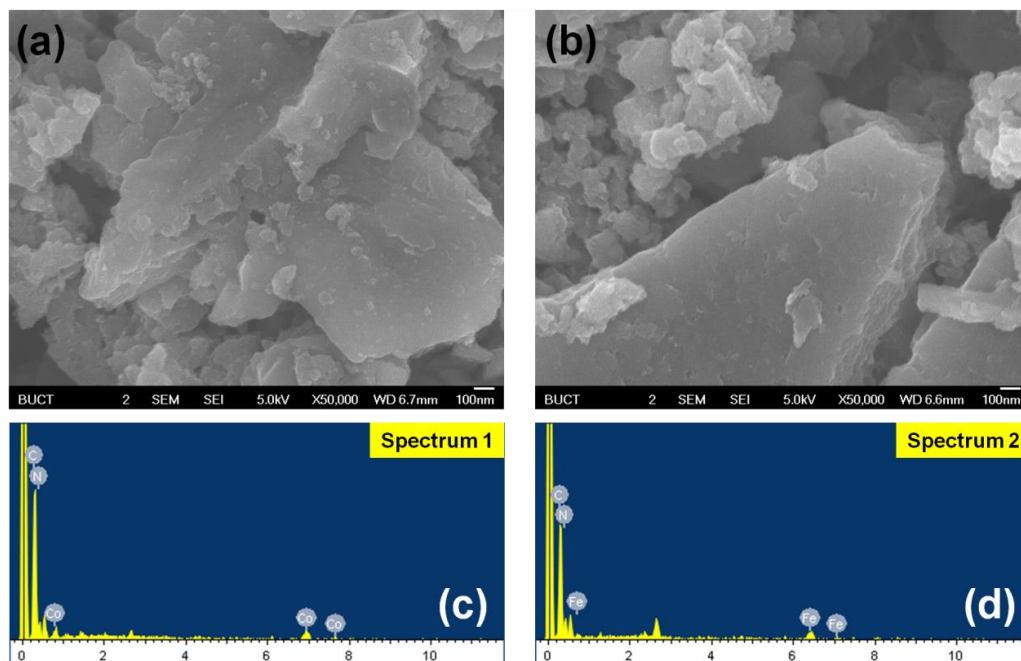


Fig. S1 SEM images of a) CoPPc-HXL, b) FePPc-HXL, and the corresponding EDS analysis of c) CoPPc-HXL, e) FePPc-HXL (unlabelled peaks is for atoms, like O, Cl).

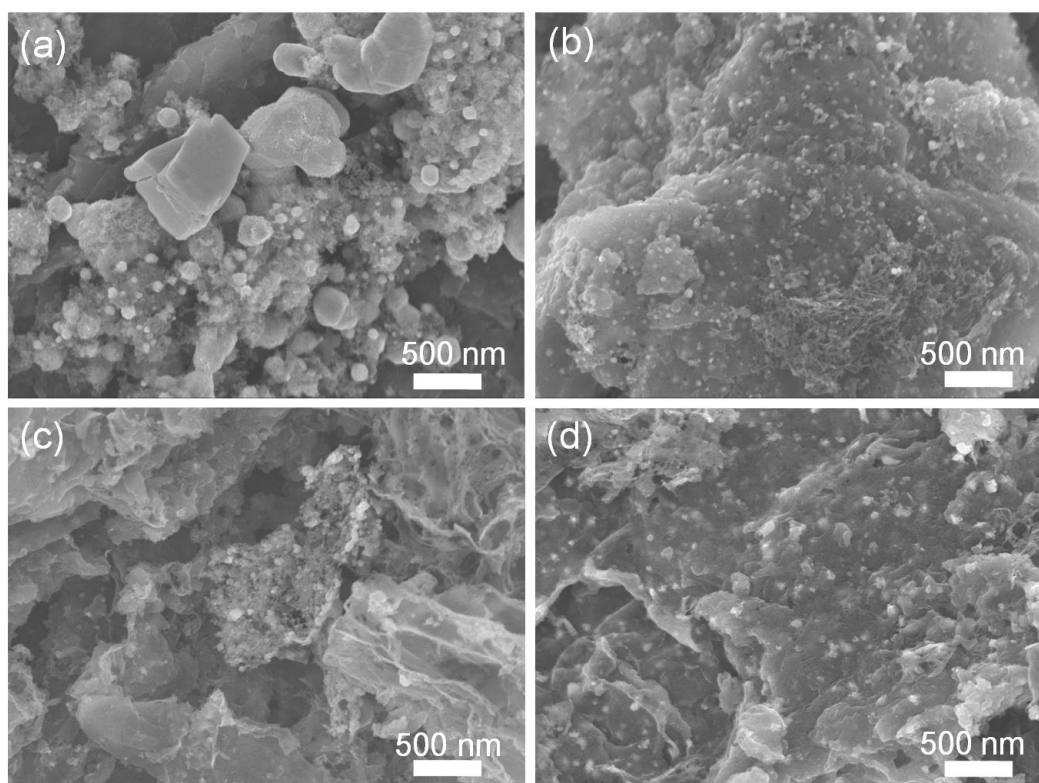


Fig. S2 SEM images of a) P-CoPc, b) P-CoPPc-HXL, c) P-CoPc and d) P-CoPPc-HXL.

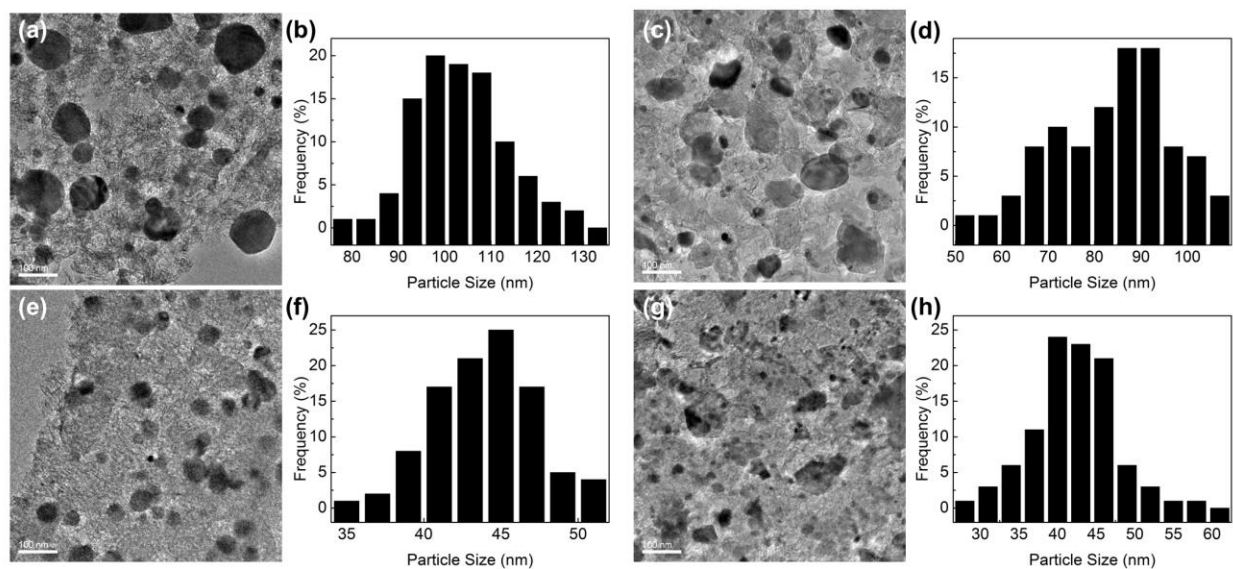


Fig. S3 TEM images of a) P-CoPPc-LXL, c) P-FePPc-LXL, e) P-CoPPc-MXL and g) P-FePPc-MXL, The figures of b), d), f) and h) showed the corresponding histogram of the particle size distribution for the above four samples, respectively.

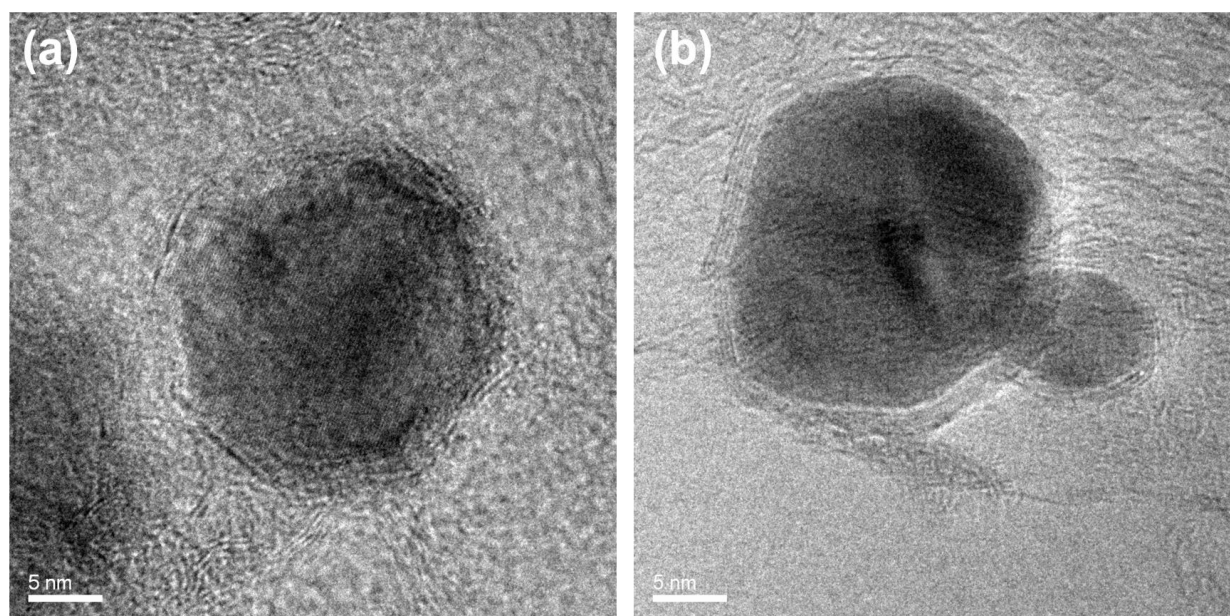


Fig. S4 High-magnification TEM images of a) P-CoPPc-HXL and b) P-FePPc-HXL.

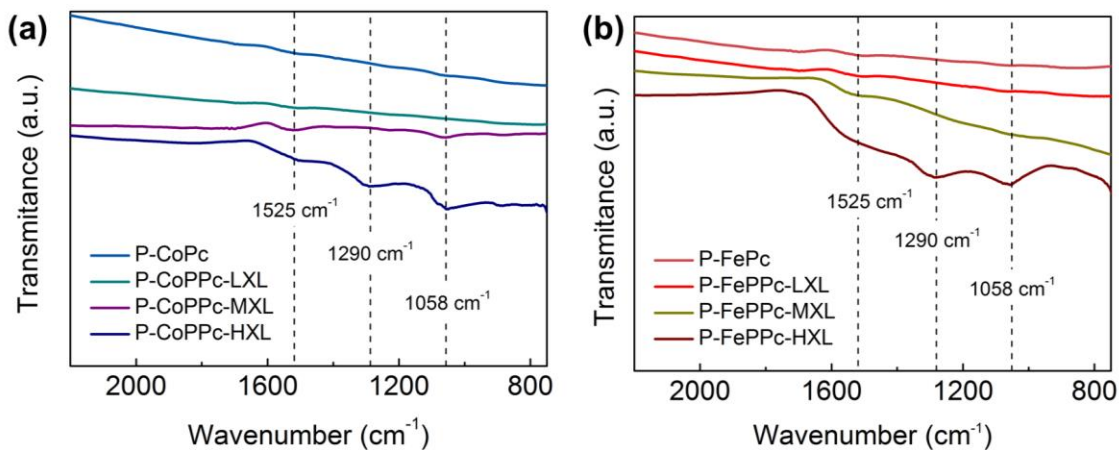


Fig. S5 FT-IR spectra of a) P-CoPc, P-CoPPc-LXL, P-CoPPc-MXL and P-CoPPc-HXL, and b) P-FePc, P-FePPc-LXL, P-FePPc-MXL and P-FePPc-HXL.

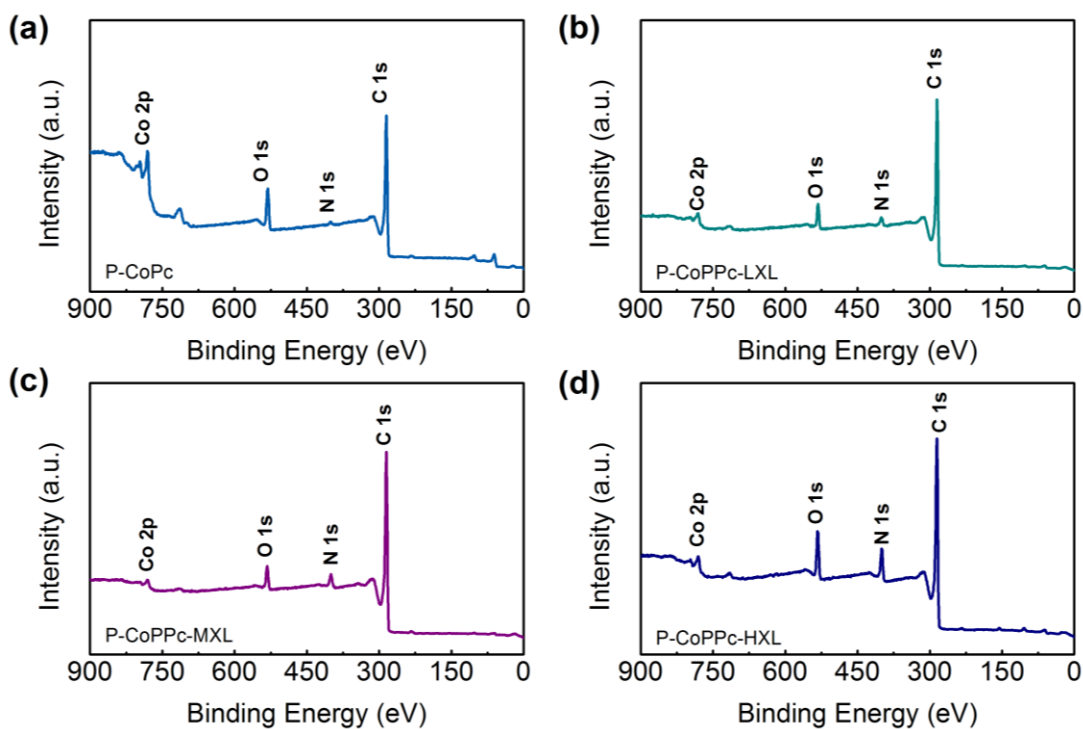


Fig. S6 XPS survey spectra of showing the elemental composition of a) P-CoPc, b) P-CoPPc-LXL, c) P-CoPPc-MXL and d) P-CoPPc-HXL.

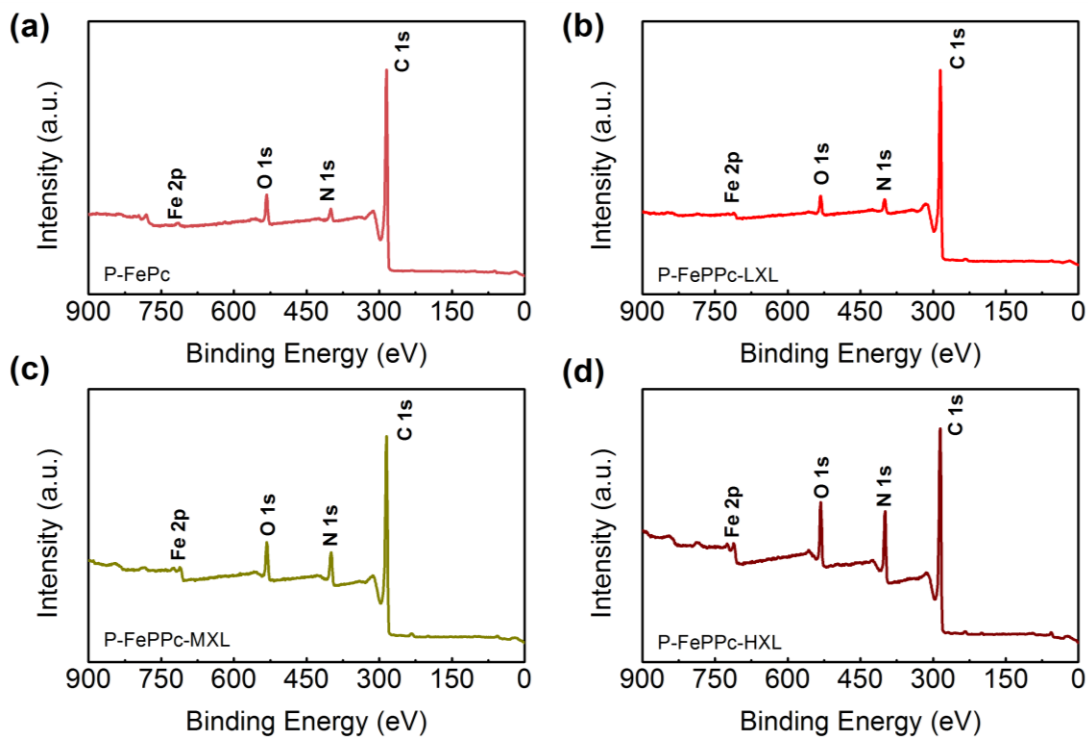


Fig. S7 XPS survey spectra of showing the elemental composition of a) P-FePc, b) P-FePPc-LXL, c) P-FePPc-MXL and d) P-FePPc-HXL.

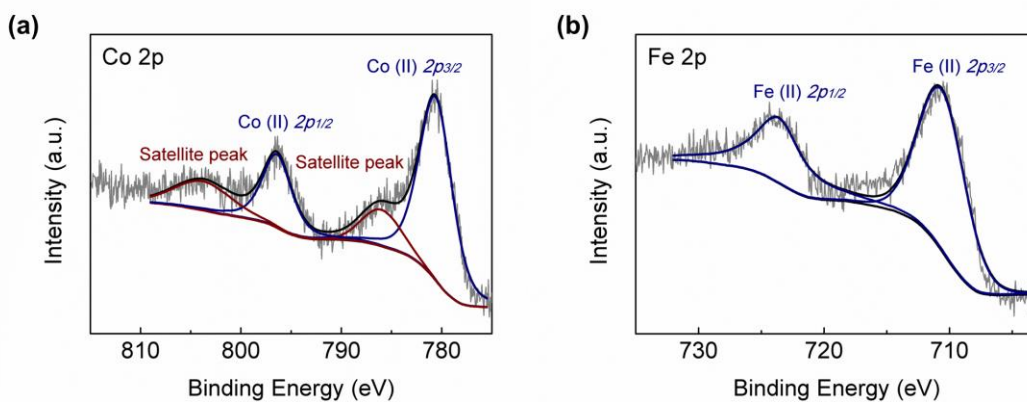


Fig. S8 XPS Co 2p and Fe 2p spectra of P-CoPPc-HXL and P-FePPc-HXL, respectively.

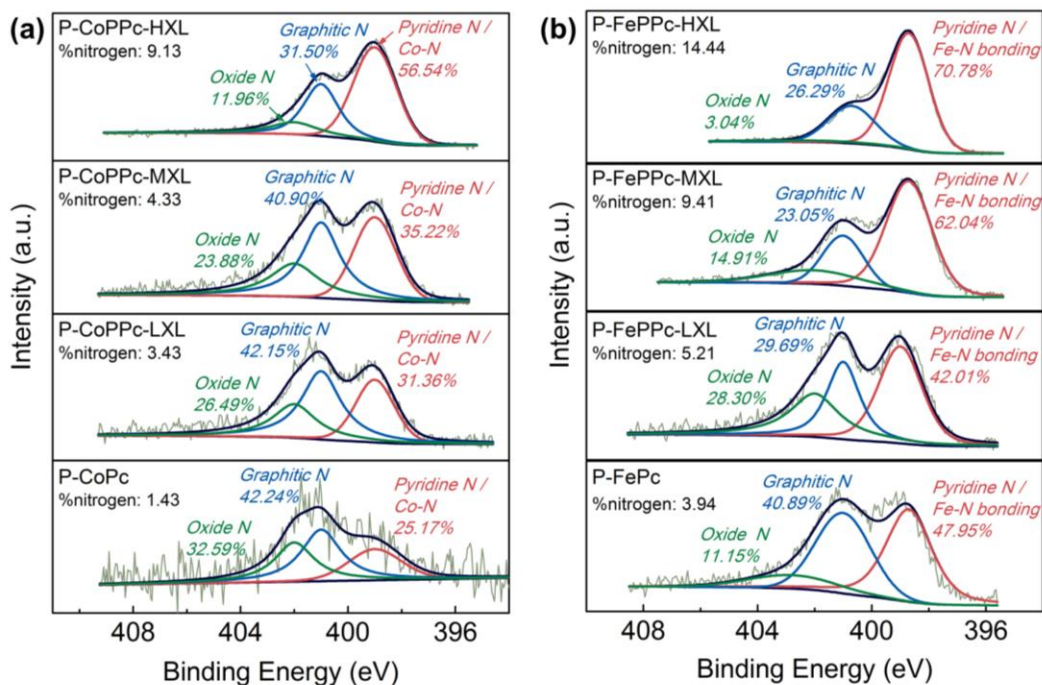


Fig. S9 XPS N 1s spectra of P-CoPc, P-CoPPc-LXL, P-CoPPc-MXL, P-CoPPc-HXL, P-FePc, P-FePPc-LXL, P-FePPc-MXL and P-FePPc-HXL. The N 1s peak can be fitted with three peaks corresponding to pyridine N and TM-N bonding (~399 eV), graphitic N (~401 eV) and oxide N (~402 eV), respectively.

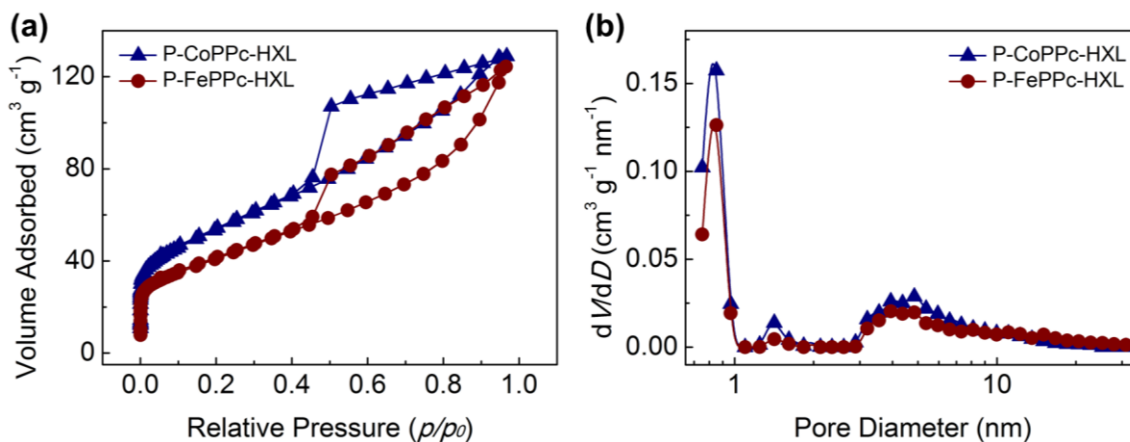


Fig. S10 BET characterization, a) N₂ adsorption–desorption isotherms and b) corresponding DFT pore size distributions for P-CoPPc-HXL and P-FePPc-HXL

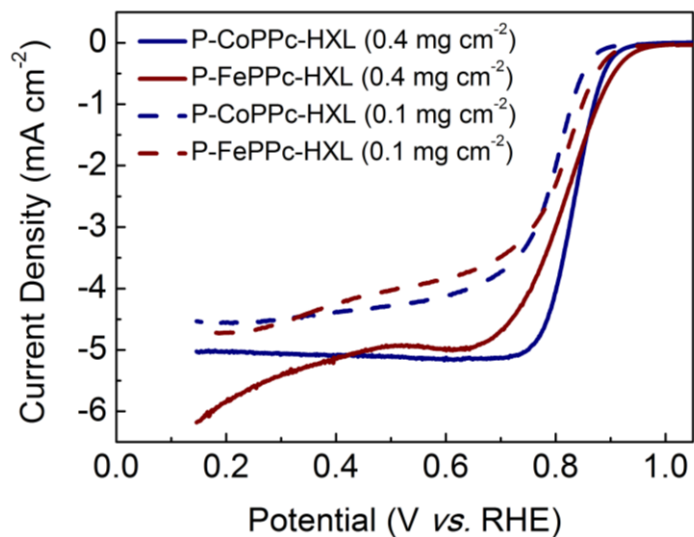


Fig. S11 Linear sweep voltammetric curves of P-CoPPc-HXL and P-FePPc-HXL with different loading mass for ORR in O₂-saturated 0.1 M KOH solution at a sweep rate of 5 mV s⁻¹ with 1600 rpm.

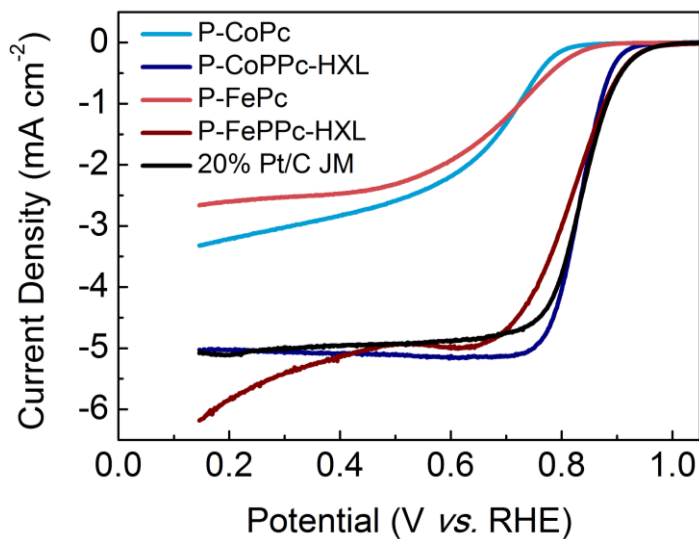


Fig. S12 Linear sweep voltammetric curves of P-CoPc, P-CoPPc-HXL, P-FePc, P-FePPc-HXL and 20%Pt/C for ORR in O₂-saturated 0.1 M KOH solution at a sweep rate of 5 mV s⁻¹ with 1600 rpm.

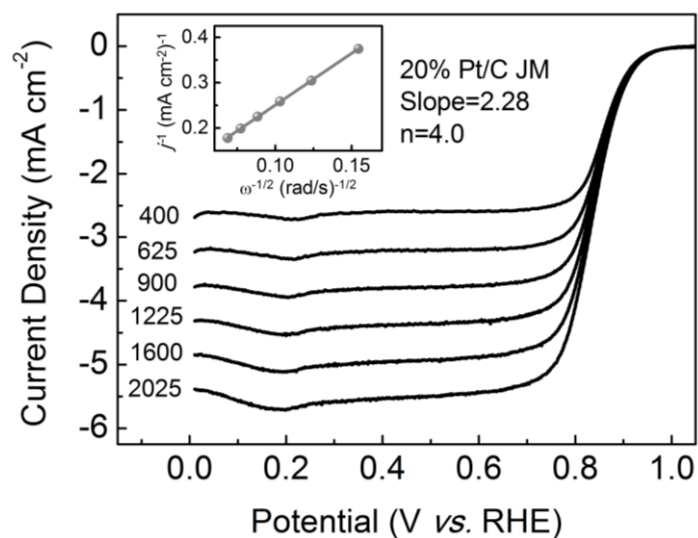


Fig. S13 Polarization curves for the electrocatalytic systems of 20% Pt/C for ORR in O₂-saturated 0.1 M KOH solution scanned at 5 mV s⁻¹ at 400-2025 rpm. The inset showed the Koutecky–Levich plots.

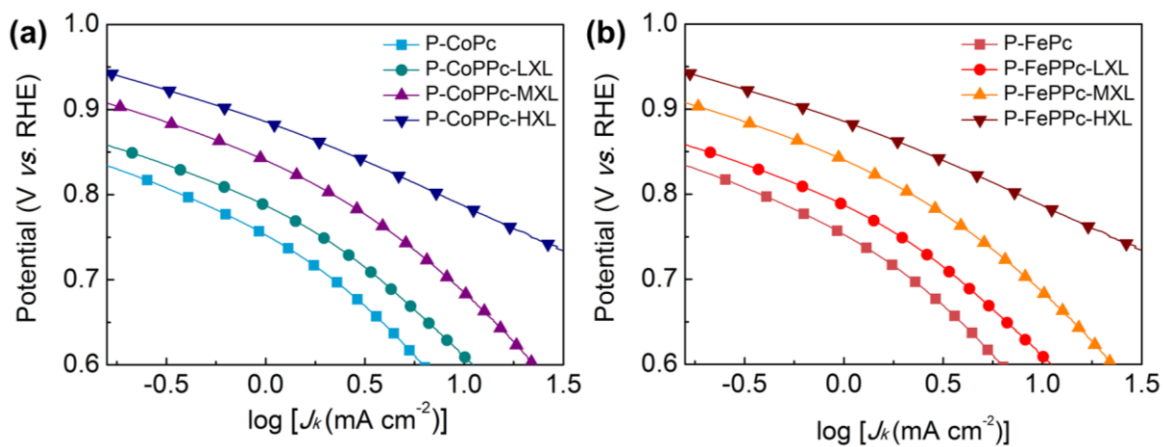


Fig. S14 Tafel plots of the a) P-CoPc, P-CoPPc-LXL, P-CoPPc-MXL and P-CoPPc-HXL, and b) P-FePc, P-FePPc-LXL, P-FePPc-MXL and P-FePPc-HXL electrodes derived by the mass-transport correction.